Positron scattering and annihilation from helium at low energies

Xian-Jun Li,[1,2] Meng-Shan Wu,[3,*] Jun Jiang,[1,†] Chen-Zhong Dong,[1] Jun-Yi Zhang,[2,‡] Zong-Chao Yan,[4,2] and Kalman Varga[5]

[1]*Key Laboratory of Atomic and Molecular Physics and Functional Materials of Gansu Province, College of Physics and Electronic Engineering, Northwest Normal University, Lanzhou 730070, China*
[2]*Innovation Academy for Precision Measurement Science and Technology, CAS, Wuhan 430071, China*
[3]*Center for Theoretical Physics, Hainan University, Haikou 570228, China*
[4]*Department of Physics, University of New Brunswick, Fredericton, New Brunswick, Canada E3B 5A3*
[5]*Department of Physics and Astronomy, Vanderbilt University, Nashville, Tennessee 37235, USA*

(Received 29 September 2023; accepted 22 November 2023; published 15 December 2023)

The confined variational method is used to study the elastic scattering of the positron from the ground-state helium with the scattering energy in the range from 0.05 eV to 11.02 eV. Describing the correlation effect with explicitly correlated Gaussians, we obtain accurate phase shifts, *S*-wave scattering length, elastic scattering cross sections, and annihilation parameters for different incident momenta. Specifically, by a least-squares fit of the data to the effective-range theory, we determine the room temperature annihilation parameter $Z_{\rm eff} = 3.955$, which is in perfect agreement with the measured result of 3.94 ± 0.02 [J. Phys. B **8**, 1734 (1975)].

DOI: 10.1103/PhysRevA.108.062816

I. INTRODUCTION

The positron, which is the antiparticle of the electron, is the most common form of antimatter. In recent years, positron experimental technology has advanced, leading to the availability of more intense positron beams [1,2]. Positrons are crucial tools in various scientific fields, including the testing of quantum electrodynamics and the standard model of particle physics [3–5], astrophysics [6], condensed matter physics [7], and medical imaging [8]. However, certain fundamental interactions of positrons with ordinary matter, such as low-energy positron annihilation and positron binding to neutral atoms and molecules, are not fully understood yet.

Positron scattering has been extensively studied for many years, both experimentally and theoretically by numerous researchers [9–26]. These studies have focused on understanding the behavior of positrons when they interact with various substances. To achieve this, sophisticated theoretical methods have been developed to account for the formation of positronium (Ps), a transient bound state of a positron and an electron. Additionally, calculations have been performed to determine the cross sections for different scattering processes. In the case of atomic and molecular targets, the positron annihilation cross section is conventionally parameterized as $\sigma_a = \pi r_0^2 (c/v) Z_{\rm eff}$, where r_0 is the classical electron radius, c the speed of light, v the incident positron velocity, and $Z_{\rm eff}$ the effective electron number participating in the annihilation process [27]. However, there exist some discrepancies between experimental annihilation values and theoretical calculations. They may be caused by various factors such as experimental uncertainties, limitations in theoretical models, or complex interactions within the studied systems. Further research and improvements are needed to resolve these discrepancies and achieve a more accurate understanding of positron scattering and annihilation processes.

The confined variational method (CVM) approach, first proposed by Mitroy *et al.* [28] and further developed by Zhang *et al.* [29], is an effective theoretical method for studying low-energy elastic scattering problems. This method has been successfully applied to various scattering systems, including e-H, e^+-H, e-He, e^+-He, Ps-H, Ps-He, and Ps-H_2 scatterings [28–34]. Recently, Wu *et al.* [31] have developed a technique that effectively addresses non-physical confinement effects, allowing the extension of CVM to non-*S*-wave scatterings at higher energies. The primary objective of this study is to extend the previous CVM calculation of e^+-He scattering by considering higher partial waves and higher scattering energies. This will provide more accurate scattering data, serving as a new benchmark for other theoretical and experimental investigations.

The rest of the paper is structured as follows. In Sec. II, a brief description of the confined variational method is given. In Sec. III, the scattering phase shifts, *S*-wave scattering length, elastic scattering cross sections, and annihilation parameters are presented. Finally, Sec. IV is a summary and outlook. The phase shifts are expressed in radians, and atomic units (a.u.) are used throughout unless otherwise stated.

II. THEORY

The theoretical method used in the present paper to study the elastic scattering of a positron from a helium atom is the CVM. Here we give a brief introduction to this method

*mswu@hainanu.edu.cn
†phyjiang@yeah.net
‡jZhang@apm.ac.cn

[28,29]. In this approach, a many-body calculation is initially conducted by incorporating a confining potential $V_{\rm cp}$ into the original Hamiltonian H of the e^+-He system. As a result, the problem is transformed into a bound-state eigenvalue problem

$$(H + V_{\rm cp})\Psi(\mathbf{r}, \mathbf{s}) = E\Psi(\mathbf{r}, \mathbf{s}), \tag{1}$$

with

$$H = -\frac{1}{2}\sum_{i=1}^{3}\nabla_i^2 + \sum_{i=1}^{3}\frac{Qq_i}{r_i} + \sum_{i<j}^{3}\frac{q_i q_j}{|\mathbf{r}_i - \mathbf{r}_j|}, \tag{2}$$

where indexes 1, 2, and 3 refer to the two electrons and the positron, respectively, q_i are their corresponding charges, and Q is the helium nuclear charge. Additionally $\mathbf{r}$ denotes collectively the coordinates $(\mathbf{r}_1, \mathbf{r}_2, \mathbf{r}_3)$ and $\mathbf{s}$ the spins $(\mathbf{s}_1, \mathbf{s}_2, \mathbf{s}_3)$. It is assumed that the nuclear mass is infinite. The eigenvalue E is the total energy of the confined scattering system, including the ground state energy of atomic helium E_0 and the scattering energy $E_s = k^2/2$, with k being the scattering momentum. The eigenfunction $\Psi(\mathbf{r}, \mathbf{s})$ is expanded in terms of the explicitly correlated Gaussian (ECG) basis [35]

$$\phi_n(\mathbf{r}, \mathbf{s}) = |\mathbf{v}|^{2K_n+L}\exp\left(-\frac{1}{2}\mathbf{r}^T A_n \mathbf{r}\right)Y_{LM}(\mathbf{v})\chi(\mathbf{s}), \tag{3}$$

where $|\mathbf{v}|^{2K_n+L}$, with K_n an non-negative integer, is the prefactor that plays a key role in describing the increasing number of nodes of the wave function, $\mathbf{v} = u^T\mathbf{r}$, with $u^T = (u_1, u_2, u_3)$ being a global vector, $\chi(\mathbf{s})$ is the spin function, A_n is a parameter matrix, Y_{LM} is the spherical harmonics, and L and M are the quantum numbers for the total orbital angular momentum and its z component, respectively. For instance, for the $L = 1$ and $k = 0.3$ case, we employ 420 basis functions for each K_n value of 0, 1, 2, 3, and 4. Consequently, the total number of basis functions used amounts to 2100.

The confining potential used here is

$$V_{\rm cp}(r_3) = \begin{cases} 0, & r_3 < R_0, \\ G(r_3 - R_0)^2, & r_3 \geqslant R_0, \end{cases} \tag{4}$$

where r_3 is the distance between the positron and helium nucleus, and R_0 is the confining radius. Moreover, R_0 is carefully selected to guarantee that the intricate short-range interaction between the positron and helium can be disregarded outside the sphere of radius R_0. In this study, the value of R_0 is chosen as $17a_0$, where a_0 is the Bohr radius.

The confining potential parameter G in Eq. (4) is tuned to ensure that a specific total energy E is yielded. With the confining potential $V_{\rm cp}$ thus constructed, we then solve the one-dimensional bound-state problem

$$\left[-\frac{1}{2}\frac{d^2}{d\rho^2} + \frac{L(L+1)}{2\rho^2} + V_m(\rho) + V_{\rm cp}(\rho)\right]\Phi(\rho) = E'\Phi(\rho). \tag{5}$$

In this step, we need to establish an adjustable model potential V_m that has the same scattering energy $E' = E_s$ under the same confining potential $V_{\rm cp}$. We choose $V_m(\rho)$ to have the form of

$$V_m(\rho) = \lambda e^{-\alpha\rho} - \frac{\alpha_d}{2\rho^4}[1 - e^{-(\rho/\beta)^6}], \tag{6}$$

where λ, α, and β are adjustable parameters, and the long-range polarization potential of the term $\sim\rho^{-4}$ is explicitly included with $\alpha_d = 1.3832$ a.u. being the polarizability of the ground-state helium [36]. In this work, we fix $\alpha = 0.5$ and $\beta = 5$, and adjust λ so that the bound-state problem Eq. (5) can yield the eigenvalue $E' = E_s = k^2/2$ for given k. Finally, the phase shift δ_L^k is determined by solving the one-dimension scattering equation for V_m

$$\left[-\frac{1}{2}\frac{d^2}{d\rho^2} + \frac{L(L+1)}{2\rho^2} + V_m(\rho)\right]\phi(\rho) = E_s\phi(\rho). \tag{7}$$

TABLE I. Convergence test of the confining parameter G, the total energy E, the positron momentum k, and the phase shift $\delta_L^k = \delta_0^{0.5}$ for the e^+-He scattering, as the size of basis set N increases. The notation $a[b]$ represents $a \times 10^b$. In atomic units.

N	G	E	k	$\delta_0^{0.5}$ (radians)
1200	1.7618605[−3]	−2.7787049	0.49999999989	−2.0764[−2]
1600	1.7618224[−3]	−2.7787190	0.49999999995	−2.0800[−2]
2000	1.7617824[−3]	−2.7787224	0.50000000014	−2.0838[−2]
2400	1.7617814[−3]	−2.7787233	0.50000000018	−2.0839[−2]
2800	1.7617813[−3]	−2.7787243	0.50000000018	−2.0839[−2]

III. RESULTS AND DISCUSSIONS

A. Phase shifts

Table I presents the convergence study of confining parameter G and δ_L^k with $L = 0$ and $k = 0.5a_0^{-1}$ as the size of basis set N increases. We can see that $\delta_0^{0.5}$ converges smoothly to fourth significant figure. In general, more basis functions are needed as k and L increase due to the increasing complexity of the wave function. In the present CVM calculations, the smallest basis set is $N = 2100$ for $\delta_0^{0.1}$ and the largest one is $N = 3600$ for $\delta_2^{0.9}$.

Table II lists the present S-, P-, D-, and F-wave phase shifts, and a comparison with various theoretical methods, including the many-body method (MBM) [24], Kohn variational method (KVM) [37], random phase shift exchange approximation (RPSEA) [38], convergent close coupling method (CCC) [39], polarized-orbital approximation method (POM) [40], and random phase approximation (RPA) [21]. The graphical comparisons of the phase shifts are given in Fig. 1. As the scattering energy increases, the S-wave phase shift reaches a maximum and eventually becomes negative. And it reaches maximum value at $k = 0.2$, which is 4.058×10^{-2} rad. The absolute values of the CVM calculations are slightly larger than the MBM ones for all the listed k. The CCC results may not be such accurate since those datas are extracted from the graphs of Ref. [39]. The CVM S-wave results are larger than the RPSEA [38] and RPA values [21] for almost all the k except for $k = 0.9a_0^{-1}$. However, there is a huge difference for $\delta_0^{0.5}$ between the POM value [40] and the CVM one. Overall, the CVM results are in good agreement with the KVM ones [37] though most of them have only two significant figures; in addition, the KVM value of $\delta_0^{0.1}$ is 6% larger.

The CVM P-wave phase shifts are converged to the third significant figure for $k = 0.1a_0^{-1}$ and $0.3a_0^{-1}$, and to the second significant figure for $0.5a_0^{-1} \leqslant k \leqslant 0.9a_0^{-1}$. Due to the difficulty of the high partial wave calculation, the CVM D-wave

TABLE II. Phase shifts for the e^+-He scattering. The notation $a[b]$ represents a $\times 10^b$. Phase shifts are in radians.

k (a.u)	CVM (this work)	MBM [24]	KVM [37]	RPSEA [38]	CCC [39]	POM [40]	RPA [21]
				S wave			
0.1	3.289[−2]	3.005[−2]	3.5(1)[−2]	2.6[−2]	−3.27[−2]	3.848[−2]	1.2[−2]
0.3	3.033[−2]	2.760[−2]	3.0(1)[−2]	1.6[−2]	−2.41[−2]	4.373[−2]	1.0[−2]
0.5	−2.084[−2]	−2.074[−2]	−2.1(1)[−2]	−3.2[−2]	−2.74[−2]	−0.428[−2]	−3.7[−2]
0.7	−8.853[−2]	−8.564[−2]	−8.9(1)[−2]	−9.1[−2]	−9.30[−2]	−7.162[−2]	−9.9[−2]
0.9	−1.583[−1]	−1.519[−1]	−1.57(1)[−1]	−1.52[−1]	−1.63[−1]	−1.418[−1]	−1.54[−1]
				P wave			
0.1	2.648[−3]	2.403[−3]	3.0[−3]	2.6[−3]	2.65[−3]	2.60[−3]	5[−4]
0.3	1.922[−2]	1.778[−2]	1.9(1)[−2]	2.0[−2]	1.85[−2]	1.920[−2]	1.1[−2]
0.5	4.03[−2]	3.795[−2]	4.1(1)[−2]	3.9[−2]	3.94[−2]	3.997[−2]	3.1[−2]
0.7	5.30[−2]	5.340[−2]	5.6(1)[−2]	5.3[−2]	5.33[−2]	5.388[−2]	4.7[−2]
0.9	5.97[−2]	6.043[−2]	6.1(1)[−2]	5.7[−2]	5.80[−2]	5.642[−2]	5.2[−2]
				D wave			
0.1	4.21[−4]	3.788[−4]	1.4[−3]	6[−4]	5.76[−4]	4.0[−4]	
0.3	3.77[−3]	3.396[−3]	4(1)[−3]	5.1[−3]	3.77[−3]	3.68[−3]	7[−4]
0.5	1.05[−2]	9.585[−3]	1.1(1)[−2]	1.16[−2]	1.04[−2]	1.025[−2]	6[−3]
0.7	2.01[−2]	1.868[−2]	2.1(2)[−2]	2.15[−2]	1.97[−2]	1.916[−2]	1.7[−2]
0.9	3.04[−2]	2.972[−2]	3.1(2)[−2]	3.2[−2]	3.06[−2]	2.842[−2]	2.9[−2]
				F wave			
0.1	1.45[−4]		1.4[−4]	2[−4]	2.35[−4]	1.3[−4]	
0.3	1.28[−3]		1.24[−3]	1.6[−3]	1.1[−3]	1.21[−3]	
0.5	3.52[−3]		4(1)[−3]	4.3[−3]	3.49[−3]	3.43[−3]	7[−4]
0.7	6.3[−3]		8(1)[−3]	8.5[−3]	6.55[−3]	6.88[−3]	4[−3]
0.9	1.2[−2]		1.2(1)[−2]	1.4[−2]	1.17[−2]	1.14[−2]	1.1[−2]

phase shifts are all converged to the second significant figure. While the the CVM F-wave phase shifts are converged to the second significant figure for $0.1a_0^{-1} \leqslant k \leqslant 0.5a_0^{-1}$, and to the first significant figure for $k = 0.7a_0^{-1}$ and $0.9a_0^{-1}$. The CVM P-, D- and F-wave phase shifts gradually increase along with the increase of k. Note that, there are significant differences between the CVM and the KVM values at $k = 0.1$ and $L = 1$ and $L = 2$. To confirm this, convergence results of CVM $\delta_1^{0.1}$ and $\delta_2^{0.1}$ have been calculated and shown in Table III and Table IV, respectively. Moreover, the KVM values of $\delta_1^{0.1}$ and $\delta_2^{0.1}$ are calculated by the formula $\delta_L^k \approx \frac{\pi\alpha k^2}{(2L-1)(2L+1)(2L+3)}$. The KVM value of $\delta_2^{0.1}$ is an order of magnitude larger than other theoretical results. The POM [40] is more effective in describing the P- and D-wave scattering than the S-wave scattering, as indicated by the results of CVM calculations. In a broader context, it becomes evident that the accuracy of the RPA values for all three partial waves falls short of that achieved by the corresponding RPSEA [38].

TABLE III. Convergence test of the confining parameter G, the total energy E, the positron momentum k, and phase shift $\delta_1^{0.1}$ (in radians) for the e^+-He scattering, as the size of basis set N increases. The notation $a[b]$ represents $a \times 10^b$. In atomic units.

N	G	E	k	$\delta_1^{0.1}$
1600	0.7209473[−5]	−2.898723757	0.09999999997	−2.9530[−2]
1800	0.7208084[−5]	−2.898724095	0.10000000000	−2.7754[−2]
2000	0.7207090[−5]	−2.898724335	0.09999999924	−2.6484[−2]
2200	0.7207086[−5]	−2.898724338	0.09999999929	−2.6478[−2]

B. S-wave scattering length

The S-wave scattering length is an important quantity that characterizes the strength of interaction between a positron and an atom at low energies. The S-wave scattering length a_s can be extracted from the effective-range expansion of the low-k scattering phase shift, written as

$$\tan\delta_0^k = -a_s k\left(1 + \frac{4\alpha_d k^2}{3}\ln k\right) - \frac{\pi\alpha_d k^2}{3} + Dk^3 + Fk^4, \tag{8}$$

where D and F are two fitting parameters. The higher-order terms have been ignored in this expansion for low-k scattering processes. To obtain an accurate scattering length, we calculate the S-wave phase shift for $0.04a_0^{-1} \leqslant k \leqslant 0.08a_0^{-1}$

TABLE IV. Convergence test of the confining parameter G, the total energy E, the positron momentum k, and the phase shift $\delta_2^{0.1}$ (in radians) for the e^+-He scattering, as the size of basis set N increases. The notation $a[b]$ represents $a \times 10^b$. In atomic units.

N	G	E	k	$\delta_2^{0.1}$
1600	0.2363711[−5]	−2.898724352	0.09999999906	4.279[−4]
1800	0.2363705[−5]	−2.898724358	0.09999999928	4.237[−4]
2000	0.2363701[−5]	−2.898724365	0.09999999943	4.209[−4]

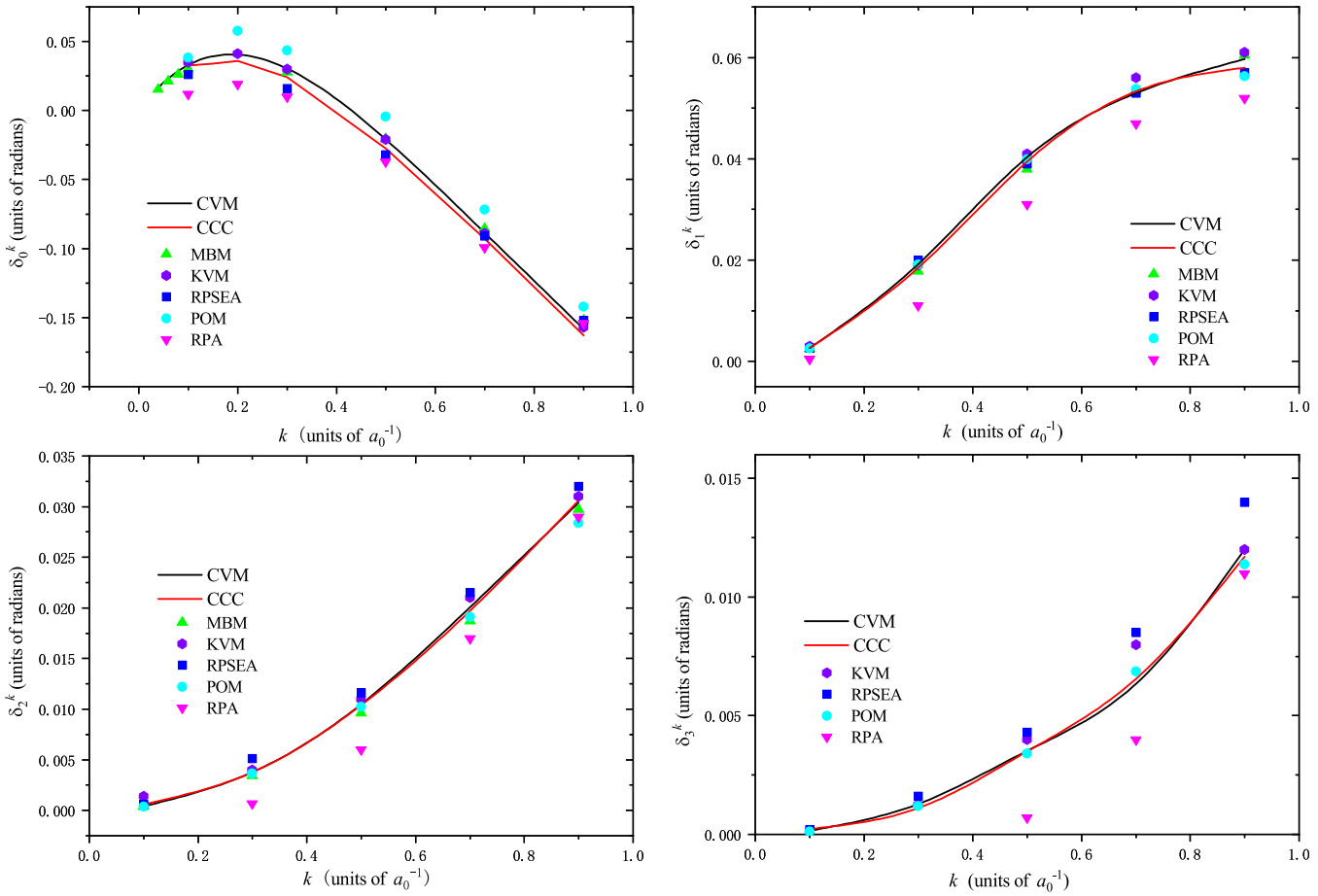

FIG. 1. Comparison of the phase shifts for S, P, D, and F wave of e^+-He scattering for $k \leqslant 0.9a_0^{-1}$. Black line for the CVM. Upper triangle for the MBM [24]. Purple hexagon for the KVM [37]. Blue Square for the RPSEA [38]. Red line for the CCC [39]. Cyan circle for the POM [40]. Pink down triangle the RPA [21].

and present the results in Table V. Figure 2 illustrates the relationship between $\tan\delta_0^k$ and positron momentum k. We determine the CVM scattering length by fitting Eq. (8). If we fit $\tan\delta_0^k$ within the range $0.05a_0^{-1} \leqslant k \leqslant 0.08a_0^{-1}$, the scattering length is found to be $a_s = -0.473a_0$. When fitting $\tan\delta_0^k$ using both $0.04a_0^{-1} \leqslant k \leqslant 0.08a_0^{-1}$ and $0.04a_0^{-1} \leqslant k \leqslant 0.07a_0^{-1}$, we obtain scattering lengths of $a_s = -0.477a_0$ and $a_s = -0.480a_0$, respectively. Taking into account the uncertainties associated with the fitting procedures, we recommend a scattering length of $a_s = -0.477a_0$. Table VI provides a comparison of scattering lengths obtained from various theoretical calculations.

TABLE V. S-wave phase shifts of the e^+-He scattering for $k < 0.1$. The notation $a[b]$ represents $a \times 10^b$. Phase shifts are in radians.

k (a.u.)	CVM (this work)	MBM [24]
0.04	1.664[−2]	1.514[−2]
0.05	2.004[−2]	
0.06	2.314[−2]	2.109[−2]
0.07	2.598[−2]	
0.08	2.855[−2]	2.606[−2]

The CVM scattering length is consistent with the SVM-stabilization value of $-0.474a_0$ [41], the KVM-5 term Hylleraas value of $-0.472a_0$ [22], the KVM-14 term

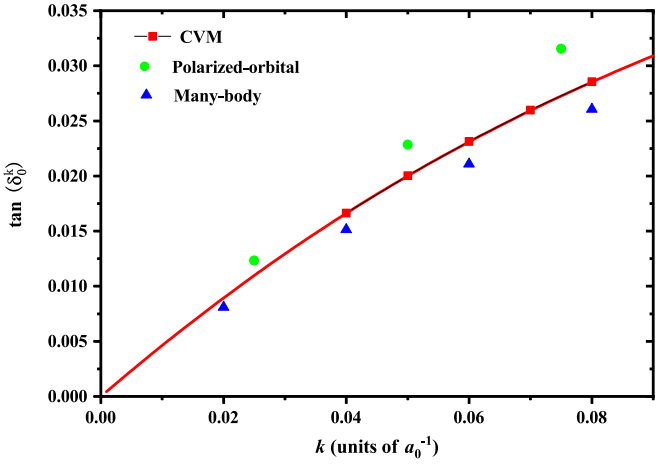

FIG. 2. S-wave phase-shift dependence on the incident positron momentum k. Blue triangles: MBM [24]; green circles: POM [40]; red squares: CVM; red solid line: the effective-range fit for $0.04a_0^{-1} \leqslant k \leqslant 0.08a_0^{-1}$ using Eq. (8).

TABLE VI. Comparison of theoretical e^+-He S-wave scattering length. In atomic units.

Method	Scattering length
CVM (this work)	−0.477
MBM [24]	−0.435
POM [40]	−0.529
KVM-5 term Hylleraas [22]	−0.472
KVM-14 term Hylleraas [42]	−0.48
KVM-22 term Hylleraas [44]	−0.50
SVM stabilization [41]	−0.474
Drachman's model B [22]	−0.524
MP [26]	−0.5017
MP [26]	−0.5056
Semi-empirical (SEM) [43]	−0.481
SVM [45]	−0.452
MP [46]	−0.45

Hylleraas value of $-0.48a_0$ [42], and the semiempirical model (SEM) value of $-0.481a_0$ [43]. It is worth noting that all three studies [22,42,44] utilize the same KVM, but they differ in the size of base set used to construct the helium wave function, which leads to slight variations in their scattering lengths. Furthermore, the CVM scattering length is approximately 9% smaller than the MBM result [24], yet it is about 10% larger than the POM result [40] and Drachman's model B result [22]. Finally, the CVM scattering length exceeds the model-potential (MP) result [26] and the KVM result [44] by approximately 6%.

C. Total cross section

The elastic total cross section is obtained as a sum over the partial waves

$$\sigma_t = \frac{4\pi}{k^2}\sum_{L=0}^{\infty}(2L+1)\sin^2\delta_L^k. \tag{9}$$

In this work, the CVM σ_t is calculated by including the CVM S-, P-, D- and F-wave phase shifts. The elastic cross sections within the framework of CVM are depicted in Fig. 3 and compared with experimental data from Stein *et al.* [9], Mizogawa *et al.* [14], Nagumo *et al.* [12], Sullivan *et al.* [13], and theoretical calculations by MBM [24], KVM [37], and SEM [43]. For ease of comparison, in Fig. 3 we also give a CVM continuous line which was obtained by fitting the selected CVM σ_t values. The CVM findings exhibit a close agreement with the experimental results of Mizogawa *et al.* [14] and Sullivan *et al.* [13] for k greater than or equal to $0.5a_0^{-1}$. However, it is noteworthy that the magnetic-field-free measurements by Nagumo *et al.* [12] yield larger values than both the corresponding theoretical predictions and other experimental observations. Comparing the CVM results with other theoretical calculations, we find a strong accord with the CCC [39], SEM [43], and KVM [37]. In contrast, the results from MBM [24] appear slightly smaller than both other theoretical predictions and experimental data for $k \geqslant 0.5a_0^{-1}$. Significant disparities emerge when examining the agreement between experimental data and theory for $k < 0.2a_0^{-1}$, though

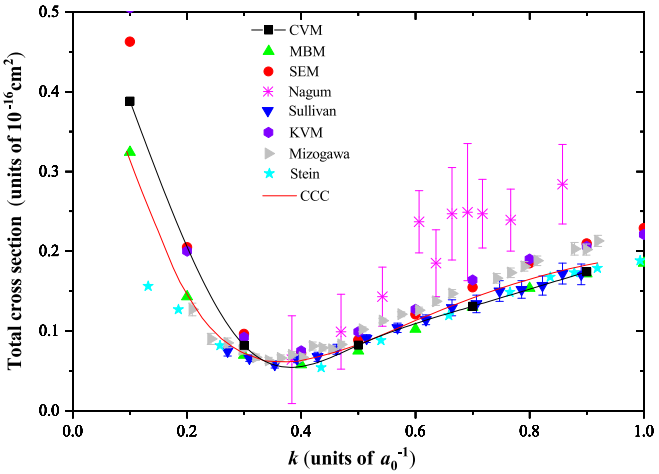

FIG. 3. Comparison of the elastic total cross sections of e^+-He scattering for $k \leqslant 0.9a_0^{-1}$. Theory: Squares for the CVM. Upper triangle for the MBM [24]. Solid circle for the SEM [43]. Hexagon for the KVM [37]. Solid line for the CCC [39]. Experiment: Stars for Stein *et al.* [9]. Right triangle for Mizogawa *et al.* [14]. Diamonds for Nagumo *et al.* [12]. Down triangle for Sullivan *et al.* [13].

the alignment of different theoretical approaches within the same k range. The precise CVM result of σ_t for $k = 0.1a_0^{-1}$ indicates a significant underestimation of the experimental values of Stein *et al.* [9].

D. Annihilation parameter

The annihilation parameter $Z_{\rm eff}$ characterizes the process of electron-positron pair annihilation that occurs during positron interacting with an atom or a molecule. In the context of a plane wave approximation, $Z_{\rm eff}$ precisely equals the number of target electrons. To gain a deeper understanding of the intricate mechanisms involved in the thermalization of positrons in gaseous environments, it becomes crucial to ascertain the energy (or temperature) dependence of $Z_{\rm eff}$. Nonetheless, the computation of $Z_{\rm eff}$ is challenging, necessitating a comprehensive consideration of electron-electron and electron-positron correlations, as well as electron exchange effects. $Z_{\rm eff}(k)$ can be calculated by the partial-wave expansion

$$Z_{\rm eff}(k) = \sum_L Z_{L,\rm eff}(k). \tag{10}$$

In the context of the e^+-He scattering scenario explored in this study, the expectation value of $\sum_{i=1}^{2}\delta(\mathbf{r}_i - \mathbf{r}_3)$ is computed using the CVM wave function

$$\langle\delta_L\rangle = \left\langle \Psi_{L,k}\left|\sum_{i=1}^{2}\delta(\mathbf{r}_i-\mathbf{r}_3)\right|\Psi_{L,k}\right\rangle, \tag{11}$$

where $\Psi_{L,k}$ is the many-body wave function in Eq. (1). This calculation is subject to the constraint of normalization. Subsequently, the ratio of the square of the confined radial wave function to the continuum radial wave function at the confinement boundary, represented by $R_0 = 17a_0$, is determined as follows:

$$\mathcal{O}_L = \frac{|\Phi(R_0)|^2}{|u_L(R_0)|^2}. \tag{12}$$

TABLE VII. Convergence test of the confining parameter G, model potention parameter λ, and the annihilation parameter $Z_{0,\mathrm{eff}}$ at $k = 0.1$. The notation $a[b]$ represents $a \times 10^b$. In atomic units.

N	G	λ	$Z_{0,\mathrm{eff}}$
1600	0.7388617[−4]	−4.43912900[−3]	3.810
2000	0.7388677[−4]	−4.68729569[−3]	3.816
2500	0.7388707[−4]	−4.44063229[−3]	3.818

Here, $\Phi(\rho)$ corresponds to the confined radial wave function as defined in Eq. (5). In order to obtain the correct value of $\Phi(R_0)$, in this step we adjust λ and α in V_{cp} of Eq. (5) so that this one-dimension bound-state problem Eq. (5) can yield the energy and normalization conditions simultaneously

$$E' = E_s,$$
$$\langle \Phi(\rho)|V_{\mathrm{cp}}(\rho)|\Phi(\rho)\rangle = \langle \Psi_{L,k}|V_{\mathrm{cp}}(r_3)|\Psi_{L,k}\rangle. \quad (13)$$

$u_L(\rho)$ is the continuum radial function which has the form

$$u_L(\rho) = (2L+1)^{1/2}\rho\big[j_L(k\rho)\cos\delta_L^k - y_L(k\rho)\sin\delta_L^k\big]. \quad (14)$$

Within this equation, $j_L(k\rho)$ and $y_L(k\rho)$ represent the spherical Bessel functions of first and second kind, respectively. Finally, the value of $Z_{L,\mathrm{eff}}(k)$ is computed according to the formula:

$$Z_{L,\mathrm{eff}}(k) = \frac{\langle\delta_L\rangle}{\mathcal{O}_L}. \quad (15)$$

The partial-wave CVM annihilation parameter $Z_{L,\mathrm{eff}}(k)$ has been calculated for different partial waves and the results are listed in Table VIII and are compared with the MBM approach [24]. As anticipated, the CVM values of $Z_{L,\mathrm{eff}}(k)$ exceed the corresponding MBM values for each k, owing to the fact that the CVM offers a more accurate representation of the short-range interaction between positron and helium, when utilizing a well-optimized ECG basis. The S-wave zero-energy annihilation parameter $Z_{0,\mathrm{eff}}^{(0)}$ is determined through a fitting procedure [47], expressed as follows:

$$Z_{0,\mathrm{eff}}(k) = Z_{0,\mathrm{eff}}^{(0)} + Z_{0,\mathrm{eff}}^{(1)}\,k^2 + Z_{0,\mathrm{eff}}^{(2)}\,k^4. \quad (16)$$

The majority of experimental data pertaining to Z_{eff} has been obtained from positrons thermalized at room temperature, where $k \sim 0.045a_0^{-1}$ [48,49]. Notably, the most precise measurement of Z_{eff} to date, which stands at 3.94 ± 0.02, was conducted by Coleman *et al.* in 1975 [49] using the time-to-amplitude converter and multichannel analyzer system. A convergence result of $Z_{0,\mathrm{eff}}$ has been given in Table VII.

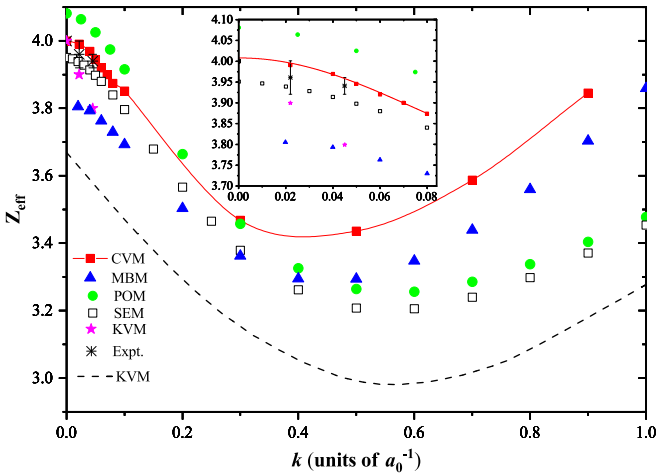

FIG. 4. Dependence of the annihilation parameter Z_{eff} on the incident momentum k for positron in helium gas. Solid square: CVM; triangle: MBM [24]; circle: POM [40]; empty square: SEM [43]; dotted line: KVM [50]; star: KVM [51]; diamonds: experiment [48,49].

In 1974, Humberston [51] performed KVM calculations of $Z_{0,\mathrm{eff}}$ and derived values of $Z_{0,\mathrm{eff}}(0) = 4.0$, $Z_{0,\mathrm{eff}}(0.022) = 3.9$, and $Z_{0,\mathrm{eff}}(0.045) = 3.88 \pm 0.01$, where $k = 0.022a_0^{-1}$ corresponds to a temperature of 77 K. Fitting $Z_{0,\mathrm{eff}}(k)$ for the range $0.04a_0^{-1} \leqslant k \leqslant 0.08a_0^{-1}$ results in $Z_{0,\mathrm{eff}}^{(0)} = 4.01$ and $Z_{0,\mathrm{eff}}(0.045) = 3.96$. Alternatively, fitting for $0.05a_0^{-1} \leqslant k \leqslant 0.08a_0^{-1}$ yields $Z_{0,\mathrm{eff}}^{(0)} = 3.99$ and $Z_{0,\mathrm{eff}}(0.045) = 3.95$. Given the uncertainties inherent in the fitting procedure, we suggest adopting the values $Z_{0,\mathrm{eff}}^{(0)} = 4.00$ and $Z_{0,\mathrm{eff}}(0.045) = 3.955$. Considering that $Z_{1,\mathrm{eff}}(k)$ for $k \leqslant 0.08a_0^{-1}$ is smaller than 3×10^{-2}, and even $Z_{2,\mathrm{eff}}(k)$ for $k \leqslant 0.08a_0^{-1}$ is considerably smaller, it is reasonable to assume that Z_{eff} is approximately equal to $Z_{0,\mathrm{eff}}$ within this range of k.

Figure 4 illustrates the relationship between Z_{eff} and positron momentum k. In the close-up view provided by Fig. 4, it becomes evident that the CVM value of $Z_{0,\mathrm{eff}}^0$ closely resembles the KVM value [51]. When the thermal temperature increases to 77 K and subsequently to 297 K, the CVM

TABLE VIII. Annihilation parameter for S-, P-, and D-wave positrons-He scattering. The notation $a[b]$ represents $a \times 10^b$.

	$Z_{S,\mathrm{eff}}$		$Z_{P,\mathrm{eff}}$		$Z_{D,\mathrm{eff}}$	
k(a.u.)	CVM	MBM [24]	CVM	MBM [24]	CVM	MBM [24]
0.04	3.969	3.788				
0.05	3.945					
0.07	3.900					
0.08	3.874	3.709				
0.1	3.818	3.660	3.286[−2]	3.233[−2]	1.046[−4]	9.235[−5]
0.3	3.161	3.079	2.999[−1]	2.764[−1]	7.151[−3]	6.976[−3]
0.5	2.656	2.569	7.257[−1]	6.779[−1]	5.416[−2]	4.714[−2]
0.7	2.261	2.186	1.157[0]	1.102[0]	1.695[−1]	1.512[−1]
0.9	1.967	1.902	1.514[0]	1.465[0]	3.638[−1]	3.366[−1]

fitting results of $Z_{\rm eff} = 3.99$ and $Z_{\rm eff} = 3.955$, respectively, fall within the error bars of accurate experimental measurements taken approximately fifty years ago. In contrast, the outcomes produced by other *ab initio* theoretical approaches, such as KVM [50] and MBM, remain out of the margins of error. On the contrary, the POM [40] overestimates $Z_{0,\rm eff}(k)$ for $k < 0.1a_0^{-1}$. This observation suggests that, from the perspective of positron annihilation, the CVM provides a more accurate description of the annihilation effect within this low-energy region.

With an increase of k, we observe a decline in $Z_{0,\rm eff}(k)$, accompanied by an increase in both $Z_{1,\rm eff}(k)$ and $Z_{2,\rm eff}(k)$ (see Table VIII). Consequently, there exists a minimum value for $Z_{\rm eff}(k)$ within the range of $0.3a_0^{-1} < k < 0.5a_0^{-1}$. For the range $0.5a_0^{-1} \leqslant k \leqslant 0.9a_0^{-1}$, when we compare the CVM-derived $Z_{\rm eff}(k)$ with results from other theoretical methods, it becomes apparent that these alternative approaches consistently underestimate the annihilation effect of the e^+-helium system.

IV. SUMMARY

The phase shifts for S, P, and D waves, total cross sections, and annihilation parameters $Z_{L,\rm eff}(k)$ have been computed for e^+-helium scattering at the positron momentum $k < 0.9a_0^{-1}$ using the CVM in conjunction with an explicitly correlated Gaussian basis. The total cross sections predicted by the CVM suggest a significant underestimation of the experimental values in Ref. [9], particularly for $k < 0.2a_0^{-1}$. Consequently, our current work will motivate further investigation from both experimental and theoretical perspectives to better understand lower energy e^+-helium scattering.

Furthermore, the CVM calculations of $Z_{L,\rm eff}(k)$ have successfully validated the precision of experimental data obtained by Coleman *et al.* [49] concerning positron annihilation in helium gas at room temperatures. Our CVM results can also serve as a benchmark for guiding future theoretical and experimental studies in this field.

ACKNOWLEDGMENTS

J.-Y.Z. is deeply indebted to S. Yi for valuable discussion and generous hospitality during his visit at the Institute of Theoretical Physics, Chinese Academy of Sciences. We thank G. F. Gribakin for helpful comments and advice. This work was supported by the National Key Research and Development Program of China under Grant No. 2022YFA1602500, the National Natural Science Foundation of China under Grants No. 12274106, No. 12174399, No. 12174316, and No. 11934014, and the Major Project of the Research Ability Promotion Program for Young Scholars of Northwest Normal University of China under Grant No. NWNU-LKQN2020-10. Z.-C.Y. was supported by NSERC of Canada.

[1] S. Schippers, E. Sokell, F. Aumayr, H. Sadeghpour, K. Ueda, I. Bray, K. Bartschat, A. Murray, J. Tennyson, A. Dorn, M. Yamazaki, M. Takahashi, N. Mason, O. Novotný, A. Wolf, L. Sanche, M. Centurion, Y. Yamazaki, G. Laricchia, C. M. Surko *et al.*, J. Phys. B **52**, 171002 (2019).
[2] S. J. Brawley, S. E. Fayer, M. Shipman, and G. Laricchia, Phys. Rev. Lett. **115**, 223201 (2015).
[3] S. G. Karshenboim, Phys. Rep. **422**, 1 (2005).
[4] A. Ishida, T. Namba, S. Asai, T. Kobayashi, H. Saito, M. Yoshida, K. Tanaka, and A. Yamamoto, Phys. Lett. B **734**, 338 (2014).
[5] The ALEPH Collaboration, The DELPHI Collaboration, The L3 Collaboration, The OPAL Collaboration, The SLD Collaboration, The LEP Electroweak Working Group and The SLD Electroweak and Heavy Flavour Groups, Phys. Rep. **427**, 257 (2006).
[6] N. Guessoum, Eur. Phys. J. D **68**, 137 (2014).
[7] F. Tuomisto and I. Makkonen, Rev. Mod. Phys. **85**, 1583 (2013).
[8] G. Jerusalem, R. Hustinx, Y. Beguin, and G. Fillet, Eur. J. Cancer **39**, 1525 (2003).
[9] T. S. Stein, W. E. Kauppila, V. Pol, J. H. Smart, and G. Jesion, Phys. Rev. A **17**, 1600 (1978).
[10] W. E. Kauppila, T. S. Stein, J. H. Smart, M. S. Dababneh, Y. K. Ho, J. P. Downing, and V. Pol, Phys. Rev. A **24**, 725 (1981).
[11] N. Overton, R. J. Mills, and P. G. Coleman, J. Phys. B **26**, 3951 (1993).
[12] K. Nagumo, Y. Nitta, M. Hoshino, H. Tanaka, and Y. Nagashima, J. Phys. Soc. Jpn. **80**, 098001 (2011).
[13] J. Sullivan, C. Makochekanwa, A. Jones, P. Caradonna, and S. Buckman, J. Phys. B **41**, 081001 (2008).
[14] T. Mizogawa, Y. Nakayama, T. Kawaratani, and M. Tosaki, Phys. Rev. A **31**, 2171 (1985).
[15] S. E. Fayer, A. Loreti, S. L. Andersen, Á. Kövér, and G. Laricchia, J. Phys. B **49**, 075202 (2016).
[16] K. Ratnavelu, M. J. Brunger, and S. J. Buckman, J. Phys. Chem. Ref. Data **48**, 023102 (2019).
[17] D. Fromme, G. Kruse, W. Raith, and G. Sinapius, Phys. Rev. Lett. **57**, 3031 (1986).
[18] S. Mori and O. Sueoka, J. Phys. B **27**, 4349 (1994).
[19] F. M. Jacobsen, N. P. Frandsen, H. Knudsen, U. Mikkelsen, and D. M. Schrader, J. Phys. B **28**, 4691 (1995).
[20] C. Wardle, J. Phys. B **6**, 2310 (1973).
[21] E. F. Varracchio, J. Phys. B **23**, L109 (1990).
[22] J. W. Humberston, J. Phys. B **6**, L305 (1973).
[23] R. P. McEachran and A. D. Stauffer, J. Phys. B **52**, 115203 (2019).
[24] D. G. Green, J. A. Ludlow, and G. F. Gribakin, Phys. Rev. A **90**, 032712 (2014).
[25] K. Strasburger, J. Phys. B **51**, 245001 (2018).
[26] A. R. Swann and G. F. Gribakin, Phys. Rev. A **101**, 022702 (2020).
[27] V. B. Berestetskii, E. M. Lifshitz, and L. P. Pitaevskii, *Quantum Electrodynamics* (Butterworth-Heinemann, Oxford, 1982), Vol. 4.
[28] J. Mitroy, J.-Y. Zhang, and K. Varga, Phys. Rev. Lett. **101**, 123201 (2008).

[29] J.-Y. Zhang, Z.-C. Yan, and U. Schwingenschlögl, Europhys. Lett. **99**, 43001 (2012).
[30] J.-Y. Zhang, M.-S. Wu, Y. Qian, X. Gao, Y.-J. Yang, K. Varga, Z.-C. Yan, and U. Schwingenschlögl, Phys. Rev. A **100**, 032701 (2019).
[31] M.-S. Wu, J.-Y. Zhang, X. Gao, Y. Qian, H.-H. Xie, K. Varga, Z.-C. Yan, and U. Schwingenschlögl, Phys. Rev. A **101**, 042705 (2020).
[32] M.-S. Wu, J.-Y. Zhang, Y. Qian, K. Varga, U. Schwingenschlögl, and Z.-C. Yan, Phys. Rev. A **103**, 022817 (2021).
[33] J.-Y. Wan, M.-S. Wu, J.-Y. Zhang, and Z.-C. Yan, Phys. Rev. A **103**, 042814 (2021).
[34] Y. Zhang, M.-S. Wu, Y. Qian, K. Varga, and J.-Y. Zhang, Phys. Rev. A **103**, 052803 (2021).
[35] J. Mitroy, S. Bubin, W. Horiuchi, Y. Suzuki, L. Adamowicz, W. Cencek, K. Szalewicz, J. Komasa, D. Blume, and K. Varga, Rev. Mod. Phys. **85**, 693 (2013).
[36] Z.-C. Yan, J. F. Babb, A. Dalgarno, and G. W. F. Drake, Phys. Rev. A **54**, 2824 (1996).
[37] P. Van Reeth and J. W. Humberston, J. Phys. B **32**, 3651 (1999).
[38] M. Y. Amusia, N. A. Cherepkov, L. V. Chernysheva, and S. G. Shapiro, J. Phys. B **9**, L531 (1976).
[39] H. Wu, I. Bray, D. V. Fursa, and A. T. Stelbovics, J. Phys. B **37**, L1 (2004).
[40] R. P. McEachran, D. L. Morgan, A. G. Ryman, and A. D. Stauffer, J. Phys. B **11**, 951 (1978).
[41] J.-Y. Zhang and J. Mitroy, Phys. Rev. A **78**, 012703 (2008).
[42] R. I. Campeanu and J. W. Humberston, J. Phys. B **10**, L153 (1977).
[43] J. Mitroy and I. A. Ivanov, Phys. Rev. A **65**, 042705 (2002).
[44] P. Van Reeth, J. W. Humberston, K. Iwata, R. G. Greaves, and C. M. Surko, J. Phys. B **29**, L465 (1996).
[45] J.-Y. Zhang and J. Mitroy, Phys. Rev. A **83**, 022711 (2011).
[46] L. A. Poveda, A. Dutra, J. R. Mohallem, and D. Assafrão, Phys. Rev. A **87**, 052702 (2013).
[47] J. Mitroy, Phys. Rev. A **66**, 022716 (2002).
[48] S. J. Tao and T. M. Kelly, Phys. Rev. **185**, 135 (1969).
[49] P. Coleman, T. Griffith, G. Heyland, and T. Killeen, J. Phys. B **8**, 1734 (1975).
[50] P. Campeanu and J. Humberston, J. Phys. B **8**, L244 (1975).
[51] J. W. Humberston, J. Phys. B **7**, L286 (1974).